

Characterization of multimode linear optical networks

Francesco Hoch,^a Taira Giordani,^a Nicolò Spagnolo,^a Andrea Crespi,^{b,c} Roberto Osellame,^c and Fabio Sciarrino^{a,*}

^aSapienza Università di Roma, Dipartimento di Fisica, Roma, Italy

^bPolitecnico di Milano, Dipartimento di Fisica, Milano, Italy

^cIstituto di Fotonica e Nanotecnologie, Consiglio Nazionale delle Ricerche, Milano, Italy

Abstract. Multimode optical interferometers represent the most viable platforms for the successful implementation of several quantum information schemes that take advantage of optical processing. Examples range from quantum communication and sensing, to computation, including optical neural networks, optical reservoir computing, or simulation of complex physical systems. The realization of such routines requires high levels of control and tunability of the parameters that define the operations carried out by the device. This requirement becomes particularly crucial in light of recent technological improvements in integrated photonic technologies, which enable the implementation of progressively larger circuits embedding a considerable amount of tunable parameters. We formulate efficient procedures for the characterization of optical circuits in the presence of imperfections that typically occur in physical experiments, such as unbalanced losses and phase instabilities in the input and output collection stages. The algorithm aims at reconstructing the transfer matrix that represents the optical interferometer without making any strong assumptions about its internal structure and encoding. We show the viability of this approach in an experimentally relevant scenario, defined by a tunable integrated photonic circuit, and we demonstrate the effectiveness and robustness of our method. Our findings can find application in a wide range of optical setups, based on both bulk and integrated configurations.

Keywords: integrated photonics; device characterization; quantum networks.

Received Aug. 4, 2022; revised manuscript received Nov. 22, 2022; accepted for publication Dec. 9, 2022; published online Jan. 3, 2023.

© The Authors. Published by SPIE and CLP under a Creative Commons Attribution 4.0 International License. Distribution or reproduction of this work in whole or in part requires full attribution of the original publication, including its DOI.

[DOI: [10.1117/1.APN.2.1.016007](https://doi.org/10.1117/1.APN.2.1.016007)]

1 Introduction

Linear optical networks are fundamental elements in several protocols for computation, communication, and sensing. Recently, many schemes for computation have found their natural implementations through optical processing, such as neuro-morphic and reservoir computing,^{1–4} optical neural networks,^{5,6} and optical simulation.^{7–9} Large-scale photonic platforms are one of the most promising candidates to implement quantum information and quantum computation protocols.^{10,11} Indeed, they have been extensively employed for quantum walks routines,^{12–14} quantum machine learning algorithms,^{15–17} and, recently, for experiments that aim at demonstrating quantum advantage with photons.^{18–20} All these protocols in classical and

quantum optics require complex interferometric structures composed of numerous optical components. Integrated photonics is one of the best candidates to realize such optical protocols in compact devices, offering, in addition, the capability to reconfigure the circuit operation.^{11,21} The latest examples of multimode optical networks^{22,23} have shown a significant increase in network complexity as well as in the number of control parameters.

The mathematical tool to model any linear optical processing in such experiments is the unitary matrix U , which describes the relation between input/output complex amplitudes of the electromagnetic field. Several relevant aspects connected to optical network programming have been identified. They range from engineering the optical setup for implementation of a given U , to the identification of universal architectures that can perform any transformation.^{24,25} Here we focus on the characterization of

*Address all correspondence to Fabio Sciarrino, fabio.sciarrino@uniroma1.it

linear optical circuits, which requires a systematic methodology to verify the operation of the optical circuit, or more generally, to reconstruct the unitary matrix implemented by the network. This task turns out to be a nontrivial one in certain scenarios. For example, interferometers based on a bulk optic implementation can be typically decomposed in elementary units that can be addressed and characterized separately. On the contrary, this procedure is typically not viable for integrated photonic circuits, and the network needs to be analyzed as a single element.

Several techniques have been developed to achieve full characterization of integrated photonic devices by exploiting different degrees of knowledge of the network's internal structure and various measurement approaches with classical or quantum light. These algorithms can be divided into two main groups. The first one is called the black-box approach and exploits only the information provided by the measurements, without assumptions on the internal structure of the optical network. The second one is the white-box approach, which exploits knowledge of the optical network structure together with the information obtained from a set of appropriately chosen measurements. White-box approaches usually make use of an optimization algorithm to estimate the parameters of the given architecture.^{26,27} It is clear that this family of reconstruction algorithms strongly depends on the knowledge of the relation between the optical component parameters and the matrix elements, and thus requires accurate modeling of the system, including noise processes. In contrast, black-box approaches aim at characterizing a multimode linear optical interferometer without using any information about its structure. They are very useful when the structure is inaccessible, untrusted, or too complex to be modeled.²³ A black box method for linear optical circuits was proposed in Ref. 28 and subsequently refined in Ref. 29. The authors presented an analytical algorithm to reconstruct the elements of the unitary matrix U from quantum light measurement, via single- and two-photon experiments. The algorithm is advantageous since it permits retrieval of matrix U even in the presence of losses and optical phase instabilities due to fiber connections in the input and output stages. However, such a method requires quantum light input states and is a slow procedure, and the accuracy is limited by noisy experimental data. In fact, the result of this reconstruction method is typically employed as a starting point for further numerical optimization to improve the stability of the solution. An alternative method exploits only classical field intensities measurements.³⁰ The moduli of the matrix elements are measured from the field intensities distribution in the output modes, while the complex phases are estimated by a measurement of the interference fringes between two coherent beams. The two procedures for the moduli and the phases estimations are independent, and they can be mapped directly onto the unitary matrix without the need to apply any further optimization algorithms.^{26,30} With this approach, a crucial requirement for a correct phase measurement is to perform the phase scan in times much shorter than the typical time scale of phase fluctuations of the system. In addition, it cannot be used in the presence of mode-dependent losses in the collection stages. Other black-box algorithms based on coherent light measurements always require high phase stability during the scan in the input and output sections,^{31–33} thus making them not viable for optical setups with in-fiber connections, which are nevertheless typical for integrated photonic devices. The last classes we mention are machine-learning algorithms,^{34,35} which need large sets of data to learn the correct transformation. Very

recently, Kuzmin et al.³⁶ simulated the application of a supervised-learning strategy for the calibration of a reconfigurable interferometer and experienced an unfavorable scaling of the training set size with the number of modes in the black-box scenario.

In this work, we propose a new black-box approach that aims at solving some open issues mentioned in the past algorithms. The goal is to provide a methodology to identify separately mode-dependent losses and matrix elements of U via coherent light measurements. In particular, we first present two algorithms to estimate the amount of loss unbalancing in the injection and collection stages of a linear optical interferometer and consequently characterize the moduli of the elements of the unitary matrix. Then we move to the problem of measuring the phases of the unitary matrix elements. Previous algorithms^{28,29} exploited second-order quantum optical correlations, such as the Hong–Ou–Mandel (HOM) effect³⁷ or the first-order classical correlations in Mach–Zehnder-like interferometric structures.³⁰ Since there are mathematical analogies between classical and quantum second-order correlations,³⁸ we propose to replace such quantities with the second-order correlations of classical light in a Hanbury Brown and Twiss-like experiment.³⁹ This approach combines some advantages of both the previous methods, i.e., the simplicity in the use of classical light³⁰ and the independence from losses and optical phase instabilities due to the fibers, characteristic of the methods that employ two-photon pairs as input states.^{28,29} Moreover, we show that the proposed classical second-order measurements depend only on the matrix phases and not on the moduli, as for the quantum correlations. This allows for completely independent estimations of the phases, input/output losses, and the moduli of the unitary matrix. From an experimental point of view, this is an important improvement that reduces the propagation of the error along the characterization process. Thus this method can be applied in a general scenario and can be effective for different experimental platforms, ranging from bulk to integrated and in-fiber optical setups.

2 Overview on Black-Box Linear Optical Circuits Reconstruction

Any ideal linear optical interferometer can be represented by a unitary matrix U , acting linearly on the annihilation (creation) operators of the electromagnetic field in the input modes a_j and transforming to the annihilation (creation) operators in the output modes b_i ,

$$b_i = \sum_j U_{ij} a_j, \quad (1)$$

where U_{ij} are the elements of the unitary matrix. The same relation holds for classical states of light, by replacing the operators a_i and b_i with the complex field E_i in Eq. (1). In other words, the elements of the unitary matrix U_{ij} completely characterize the field amplitudes' propagation through a multimode optical network. In general, the set of optical modes i may represent any degree of freedom of light, such as polarization, path, time of arrival, frequency, angular, and transverse momentum.

Optical losses deviate the interferometer operation from the unitarity. To take into account the losses, we consider biased insertion losses at the input and at collection stages and balanced

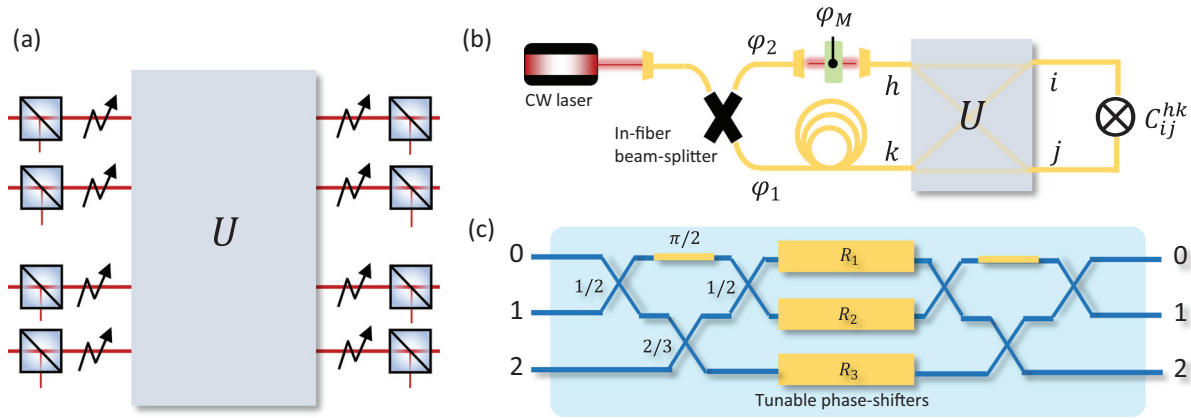


Fig. 1 Reconstruction of multimode optical circuits. (a) Model of a multimode interferometer considered in this work. It is composed by the ideal optical circuit described by the unitary transformation U plus layers of mode-dependent losses at the input and at the output (represented by beam splitters) and phase instabilities (represented by sparks). Output losses take into account also possible differences in the detection efficiencies among the modes. (b) Scheme for the measurement of second-order cross-correlations C_{ij}^{hk} with coherent light emitted by a CW laser. The latter is coupled in single-mode fiber and split into two beams by an in-fiber beam splitter. The two beams enter the interferometer in modes h, k . The phase modulation φ_M performed by a liquid crystal compensates for the fiber phase fluctuations $\varphi = \varphi_1 - \varphi_2$ to satisfy the conditions in Eq. (17). (c) The three-mode integrated chip employed to test the reconstruction algorithm. It is composed of a sequence of two tritter structures. Each tritter comprises three beam splitters, whose reflectivity is reported in this figure, and a phase-shift equal to $\pi/2$. Between the two tritters, there are three heaters $\{R_1, R_2, R_3\}$ that dynamically control the optical phases between the two structures via the thermo-optic effect.

internal losses, which are known to commute with the unitary matrix.⁴⁰ This assumption is not the most general, since it considers the optical transformation U without any internal imbalances among the modes. Currently, most of the photonic circuits are designed in such a way that losses are practically unbiased along the evolution and can be factorized to one of the ends of the interferometer.²⁵ Then our model of losses can find applications in many scenarios. We model losses as shown in Fig. 1(a) with a set of beam splitters placed on the input and output modes. We further consider the presence of unknown (and possibly unstable) phase terms on these modes. The device is thus described by a matrix $T = \mathcal{D}_1 U \mathcal{D}_2$, where \mathcal{D}_1 and \mathcal{D}_2 are diagonal matrices that account for such losses and additional phases. The matrix elements of the unitary part are expressed as $U_{ij} = \tau_{ij} e^{i\phi_{ij}}$, where τ_{ij} and ϕ_{ij} are the matrix moduli and phases, respectively. In what follows, we briefly analyze the two most general algorithms in the literature to reconstruct the matrix U . The first algorithm exploits quantum light,²⁸ and the second one is based on coherent light measurements.³⁰

If one employs measurements with Fock states at the input of the interferometer and photon-number-resolving detection at the output, the results will be insensitive to the (unstable) phase terms at the input and at the output. This means that the matrix U and all the matrices U' in the form $U' = F_1 U F_2$, where F_1 and F_2 are unitary diagonal matrices, and are equivalent. Another invariance property of these measurements carried out with Fock states is that the outcomes do not change with respect to the conjugate operation $U' = U^*$. Given these equivalence relations, it is not necessary to reconstruct the actual unitary matrix implemented by the interferometer, but only a representative element of its class of equivalence. This is commonly defined by

choosing a matrix with real-valued elements in the first row and first column ($\phi_{0i} = 0$ and $\phi_{i0} = 0$) together with the condition that the element U_{11} has positive phase ($\phi_{11} > 0$). Laing and O'Brien²⁸ presented an algorithm to reconstruct the value of moduli and phases of the representative unitary matrix elements via single-photon intensity and two-photon measurements, the latter via the visibility \mathcal{V} of HOM interference.³⁷ Labeling the input modes of the two photons as h, k , and the output ones as i, j , the visibility is defined as

$$\mathcal{V}_{ij}^{hk} = 1 - \frac{(P_{ij}^{hk})^I}{(P_{ij}^{hk})^D} = \frac{-2\tau_{jk}\tau_{ih}\tau_{ik}\tau_{jh}}{\tau_{jk}^2\tau_{ih}^2 + \tau_{ik}^2\tau_{jh}^2} \cos(\phi_{jk} + \phi_{ih} - \phi_{ik} - \phi_{jh}), \quad (2)$$

where $(P_{ij}^{hk})^I$ is the probability to find the two (indistinguishable) photons in output modes (i, j) when they are injected, respectively, in input modes (h, k) , whereas $(P_{ij}^{hk})^D$ correspond to the same quantity with distinguishable particles. Note that the visibility \mathcal{V} does not change in the presence of mode-dependent losses in both preparation and measurement stages, and thus its estimation gives direct access to the matrix elements. By measuring these quantities, it is possible to define a system of equations and to retrieve an analytical solution to the problem, as shown in Refs. 28 and 29. One of the main constraints of such an approach is the requirement of measurement with quantum light. Recently, a further method that exploits quantum light probes, such as two-mode squeezed states, and single-photon counting combined with heterodyne measurements, provided

further refinement for reconstructing the U matrix in the presence of internal unbalanced losses.⁴¹

The other method proposed in Ref. 30, based on classical intensity measurements, requires phase stability within the measurement time to estimate matrix phases, since these values are extracted from first-order correlation functions. This means that in such a measurement scheme, the equivalence between U and U' does not hold. Additionally, the correct estimation of matrix element moduli, which in this approach is performed independently from the phase estimations, is spoiled by the presence of output mode-dependent losses.

3 Algorithm for Reconstruction of Linear Interferometers

In this section, we propose an alternative black-box methodology based on coherent light probes. This approach permits the estimation of matrix elements moduli and losses also in the presence of loss imbalance among the modes and retrieving quantities having the same properties of \mathcal{V} without requiring phase stability at the inputs and outputs of the interferometer.

3.1 Reconstruction of Moduli and Losses

We start our investigation with the estimation of the matrix elements moduli τ_{ij} . The τ_{ij}^2 coefficients represent the probability of finding a single photon in output mode j given an input mode i or, alternatively, the fraction of classical field intensity in the mode j . This observation allows one to define a probability matrix $P_{ij} = \tau_{ij}^2$. The main task is to estimate such a matrix when mode-dependent losses are present in the preparation and collection stages. Let us define M as the matrix obtained from single-mode intensity measurements, estimated experimentally via single-photon input states or by injecting laser light in a single mode. Following the model presented in Fig. 1(a), the actual measured matrix M can be expressed as

$$M = D_1 P D_2, \tag{3}$$

where D_1 and D_2 are the diagonal matrices that describe the unbalanced losses in input and output modes. The task then requires reconstructing the probability matrix P and the input and output losses matrices D_1 and D_2 starting from the measured matrix M . To this end, we now introduce below two approaches that can be used to estimate D_1 and D_2 up to a multiplicative factor and, consequently, matrix P under very few assumptions on the measured matrix M .

3.1.1 Sinkhorn's decomposition-based algorithm

A first approach to reconstruct matrices P , D_1 , and D_2 is obtained starting from the observation that the probability matrix P is a doubly stochastic matrix, i.e., the matrix has nonnegative entries and the sum of each row and each column is equal to 1. It is thus possible to apply Sinkhorn's theorem and the matrix scaling algorithm on this system.^{42,43} Indeed, a matrix with nonnegative elements such as M admits a Sinkhorn's decomposition if it is diagonally equivalent to a doubly stochastic matrix, i.e., can be written in the form $D_1 P D_2$, where D_1 and D_2 are the diagonal matrices and P is a doubly stochastic matrix. This decomposition exactly represents the solution to our problem [see Eq. (3)]. Sinkhorn's theorem and subsequent extensions⁴² guarantee that this solution exists and it is unique. The theorem gives us also an important warning, since the algorithm is

sensitive to the position of the zero elements of the measured matrix M . This means that an incorrect attribution of zero-valued elements in M , due to experimental errors or limited measurement sensitivity, could make the matrix impossible to decompose with Sinkhorn's theorem.

Finding Sinkhorn's decomposition for a nonnegative matrix M is a special case of the matrix scaling problem that has applications in a large variety of fields. In our case, defining $X = D_1^{-1}$ and $Y = D_2^{-1}$, we can write $P = XMY$ and using the property that P has to be doubly stochastic, we obtain the following system of equations:

$$\begin{cases} XMY\vec{e} = \vec{e}, \\ YM^T X\vec{e} = \vec{e}, \end{cases} \tag{4}$$

where \vec{e} is the vector with all the components equal to 1.

In the literature, different algorithms have been proposed to solve Eq. (4). Here we present a specific choice among the possible algorithms (see Ref. 44 for a review of the possible approaches). The chosen algorithm allows the recovery of all three matrices in Eq. (3). The idea is to rearrange Eq. (4) in terms of vectors \vec{x} and \vec{y} , which are the diagonal elements of X and Y . Formally, they can be expressed as $\vec{x} = X\vec{e}$ and $\vec{y} = Y\vec{e}$. By defining the inversion of a vector as the inversion component-by-component, $\vec{x}^{-1} = (x_1^{-1}, x_2^{-1}, \dots, x_N^{-1})^T$, we find that

$$\begin{cases} \vec{x} = (M\vec{y})^{-1}, \\ \vec{y} = (M^T\vec{x})^{-1}. \end{cases} \tag{5}$$

At this point, we apply an iterative algorithm to solve the system of Eq. (5) and retrieve the two vectors \vec{x} and \vec{y} and, consequently, the two diagonal matrices X and Y . Then we can recover the probability matrix $P = XMY$ and the two loss matrices as $D_1 = X^{-1}$ and $D_2 = Y^{-1}$.

3.1.2 Variance-minimization-based algorithm

In the derivation of the previous algorithm to solve Eq. (3), we have implicitly assumed to have measured the field intensity distribution for any combination of outputs j for any input i . In the following method, we define an alternative procedure that can be applied when only a subset of the inputs is available, while requiring the capability of reconfiguring the linear optical network.

Let us then consider an interferometer, in which it is possible to change the probability matrix P without affecting the input and output losses D_2 and D_1 and to measure all the output configurations only for a subset of input modes. We first consider the scenario, in which the light source, a single photon, or a laser beam, is injected only in mode i . In the absence of unbalanced losses, the outcome \vec{M} of such intensity measurements is proportional to the vector \vec{P}_i , (the i 'th column of the matrix P) and represents a discrete probability distribution that depends from a set of parameters $\vec{\theta}$ describing the optical circuit settings. By taking into account the presence of unbalanced losses \vec{D} (D_1 in the general case), the components M_j of vector \vec{M} are

$$M_j(\vec{\theta}) = I P_j(\vec{\theta}) D_j, \tag{6}$$

where I is the intensity attenuated by the input loss. Since we are injecting light in the same mode for all measurements, this factor can be included in \vec{D} .

The separation of the probability from the losses in Eq. (6) can be done starting from the following observation. Let us define the quantity $S(\vec{\alpha}, \vec{\theta})$ as the weighted sum of the components of \vec{M} ,

$$S(\vec{\alpha}, \vec{\theta}) = \sum_j \alpha_j M_j(\vec{\theta}). \quad (7)$$

If the vector of the weights $\vec{\alpha}$ is proportional to the element-wise inverse of the losses vector \vec{D} , the quantity S does not vary with the control parameter $\vec{\theta}$. In fact, when $\vec{\alpha} = \beta \vec{D}^{-1}$, where β is a global factor, we have

$$S(\beta \vec{D}^{-1}, \vec{\theta}) = \beta \sum_j D_j^{-1} M_j(\vec{\theta}) = \beta \sum_j D_j^{-1} D_j P_j(\vec{\theta}) = \beta. \quad (8)$$

In general, $S(\vec{\alpha}, \vec{\theta})$ changes with the control parameters $\vec{\theta}$. Then the idea is to find the weight vector $\vec{\alpha}$ such that $S(\vec{\alpha}, \vec{\theta})$ is constant when the control parameters $\vec{\theta}$ vary. This vector can be obtained by minimizing the variance of $S(\vec{\alpha}, \vec{\theta})$ with respect to $\vec{\alpha}$. The variance $\xi^2(\vec{\alpha})$ can be estimated on a sufficiently large set of settings of the parameters $\{\vec{\theta}_i\}$ as

$$\xi^2(\vec{\alpha}) = \frac{\sum_{i=0}^{n-1} S(\vec{\alpha}, \vec{\theta}_i)^2}{n} - \left(\frac{\sum_{i=0}^{n-1} S(\vec{\alpha}, \vec{\theta}_i)}{n} \right)^2, \quad (9)$$

where n is the number of different settings $\{\vec{\theta}_i\}$, and consequently represent the size of the measurement outcome vector $\{\vec{M}(\vec{\theta}_i)\}$. This minimization is equivalent to a quadratic optimization problem. To solve such a task, let us call $\mathcal{M}_{ij} = [\vec{M}(\vec{\theta}_i)]_j$ the matrix in which each row contains the output intensities distribution for a particular configuration of the chip; then we define the following positive semidefinite matrix Q as

$$Q_{hk} = \frac{1}{n} \sum_{i=0}^{n-1} \mathcal{M}_{ih} \mathcal{M}_{ik} - \frac{1}{n^2} \sum_{i=0}^{n-1} \sum_{j=0}^{n-1} \mathcal{M}_{ih} \mathcal{M}_{jk}. \quad (10)$$

Then our problem can be rewritten, in terms of the matrix Q , as

$$\xi^2(\vec{\alpha}) = \sum_i \sum_j Q_{ij} \alpha_i \alpha_j. \quad (11)$$

The minimization of Eq. (11) has as a trivial solution $\vec{\alpha} = \vec{0}$ (the vector with all null components) and another one that is the eigenvector of Q corresponding to a null eigenvalue. The latter solution corresponds exactly to the element-wise inverse of the losses vector $\vec{\alpha} = \vec{D}^{-1}$. In the presence of noisy experimental data, the solution is the eigenvector of Q corresponding to the lowest eigenvalue. Alternatively, the nontrivial solution can be found by an ordinary numerical minimization approach of Eq. (11). This can be fulfilled by setting a normalization constraint $\vec{N} \cdot \vec{\alpha} = 1$ for some normalization vector \vec{N} , since losses can be estimated with this procedure up to a multiplicative factor common to all the modes.

The method can be generalized to the scenario, in which one is interested in reconstructing a submatrix of P . Then it is possible to reconstruct even the relative losses between the different measured input modes. Here we suppose a set of output vectors

$\{\vec{M}_i\}_k$ for each input $k \in K$ and compute the variance function $\xi_k^2(\vec{\alpha})$ and the associated matrix $Q^{(k)}$. At this point, we minimize the sum of all variances with the same constraints of the previous derivation,

$$\sum_{k \in K} \xi_k^2(\vec{\alpha}) = \sum_i \sum_j \sum_{k \in K} Q_{ij}^{(k)} \alpha_i \alpha_j. \quad (12)$$

After the minimization, it is possible to recover the input losses from the value of the sum function associated with each input as follows:

$$\frac{(\vec{D}_2)_k}{(\vec{D}_2)_{k'}} = \frac{\frac{1}{n} \sum_{i=0}^{n-1} \sum_j \alpha_j \mathcal{M}_{ij}^{(k)}}{\frac{1}{m} \sum_{i=0}^{m-1} \sum_j \alpha_j \mathcal{M}_{ij}^{(k')}}. \quad (13)$$

3.2 Reconstruction of the Internal Phases with Classical Light

Here we propose a procedure to estimate the complex phases of the matrix elements ϕ_{ij} . The methods reported in Refs. 28 and 29 employ the visibility of the HOM effect described in Eq. (2) for this task, by sending a two-photon input state whose indistinguishability is tuned during the experiment. In this work, we propose an analogous quantity that can be measured by intensity cross-correlation at the output of the linear network with classical light. The measurement scheme is presented in Fig. 1(b). The laser source is split and sent into the network in modes (h, k) . The additional phases φ_1 and φ_2 account for phase instabilities in the optical paths between the sources and the interferometer. We can define the cross-correlation σ_{ij}^{hk} between the output modes (i, j) when the two beams enter from modes (h, k) as

$$\sigma_{ij}^{hk} = \langle (I_i - \langle I_i \rangle)(I_j - \langle I_j \rangle) \rangle = \langle I_i I_j \rangle - \langle I_i \rangle \langle I_j \rangle, \quad (14)$$

where I_i and I_j are the field intensities in the corresponding output modes, whereas $\langle \cdot \rangle$ is the time average. We define also the self-correlation σ_{ii}^{hk} of the intensity fluctuation as

$$\sigma_{ii}^{hk} = \langle (I_i - \langle I_i \rangle)^2 \rangle = \langle I_i^2 \rangle - \langle I_i \rangle^2. \quad (15)$$

We make the hypotheses that (i) the external phase fluctuations $\varphi = \varphi_1 - \varphi_2$ have zero time average and (ii) the input laser intensity is constant. After some calculations, reported in Sec. II in the [Supplementary Material](#), we can define the normalized cross-correlation C_{ij}^{hk} as

$$C_{ij}^{hk} = \frac{\sigma_{ij}^{hk}}{\sqrt{\sigma_{ii}^{hk} \sigma_{jj}^{hk}}} = \cos(\phi_{ih} - \phi_{ik} - \phi_{jh} + \phi_{jk}). \quad (16)$$

Note that this quantity only depends on the phase of the matrix elements. Similar to HOM visibility in two-photon experiments, the set $\{C_{ij}^{hk}\}$ does not depend on the input and output losses. Additionally, and at variance with HOM visibility, $\{C_{ij}^{hk}\}$ does not depend also on the moduli $\{\tau_{i,j}\}$ of the matrix elements, thus permitting an independent estimation of the phases. The derivation of Eq. (16) is performed under a specific

assumption on the external optical phase fluctuations at the input. More specifically, we require that

$$\langle e^{i\varphi} \rangle = 0 \quad \langle e^{2i\varphi} \rangle = 0. \quad (17)$$

In general, mechanical and thermal phase fluctuations do not satisfy these conditions. These equations can be satisfied by adding a phase modulator in one of the two input paths. In this scenario, the external phase contribution can be expressed as $\varphi = \varphi_M + \varphi_T$, where φ_M is the modulated phase and φ_T is the one modified by thermal and mechanical noise. Since the two contributions are uncorrelated, we can write $\langle e^{i\varphi} \rangle = \langle e^{i\varphi_M} \rangle \langle e^{i\varphi_T} \rangle$. Controlling the phase modulation such that $\langle e^{i\varphi_M} \rangle = 0$ and $\langle e^{2i\varphi_M} \rangle = 0$, for example, by adding white noise with appropriate amplitude or by a discrete set of phases, the conditions of Eq. (17) can be satisfied.

3.3 Complete Algorithm

Given the methods defined above, we can summarize the complete procedure to reconstruct the matrix U as follows:

1. Perform field intensity measurements in the output of the circuit. Apply the Sinkhorn-based algorithm to retrieve the complete set of moduli for the matrix elements ($\{\tau_{i,j}\}$) or the variance minimization approach to estimate a specific subset.
2. Perform cross-correlation measurements in pairs of the output of the circuit. Solve the system of equations for the set $\{C_{ij}^{hk}\}$ to extract the complex phases of the unitary matrix.

Note that point 2 has some similarities to the procedure proposed in Refs. 28 and 29 with HOM visibilities. In particular, this approach could require a further minimization step on a larger set of $\{C_{ij}^{hk}\}$ with respect to the minimum ensemble needed to solve the system. Nonetheless, it is worth noting that, in our case, we do not require (i) the use of indistinguishable single-photon states and (ii) the measurements of $\{C_{ij}^{hk}\}$ give us directly the information about the phases without requiring the knowledge of the matrix moduli. In fact, in our algorithm, points 1 and 2 are independent, as for the previous methods with coherent probe light,^{30,33} but have the additional features of permitting the estimation of losses. Furthermore, it can be applied in any scenario with phase instabilities.

4 Experimental Verification in a Reconfigurable Integrated Circuit

We tested the complete algorithm described in the previous section in a three-mode reconfigurable optical circuit. The waveguides of the device were fabricated in a glass sample via the femtosecond laser-writing technique⁴⁵ (see Sec. III in the [Supplementary Material](#) for more details). The structure is composed of a sequence of two tritters, a circuit that generalizes the beam splitter over three modes^{46,47} [see also Fig. 1(c)]. Between the two tritters, the presence of three resistive heaters permits the change of the unitary transformation performed by the circuit via the thermo-optic effect. The measurements were performed with a continuous-wave (CW) laser at the wavelength of $\lambda = 785$ nm. The laser is routed in different input modes via a fiber switch connected to a fiber array that injects light into the input port of the interferometer. The field intensity distribution in the three output ports was recorded via a CCD camera.

Our first experimental test regards the two algorithms described above, to retrieve the losses vectors and moduli of

the matrix elements. In Figs. 2(a) and 2(b), we report the results for the application of Sinkhorn's decomposition method. In particular, in (a), we report the measured field intensity M for a particular configuration of the chip, normalized to the column total intensity. Here we inserted on-purpose additional losses by placing an attenuation filter on the output mode 0, to test the performances of the approach. In Fig. 2(b), we report the probability matrix P after the applications of the Sinkhorn algorithm. We measured the moduli of a set of N different transformations U , each of them in two loss conditions, namely, by inserting and removing the attenuation filter in mode 0. Defining the fidelity as $F = (1/3 \sum_{i,j=0}^2 \sqrt{P_{ij}P'_{ij}})^2$, the average classical similarity between the two reconstructed distributions in the two losses configurations for a given U via the Sinkhorn method is $F = 0.9999 \pm 0.0001$ ($F_{\min} = 0.9997$). The average was estimated on the set of the N pairs of matrices. This confirms that the method works properly in different mode-dependent loss configurations and retrieves, as expected, always the same moduli $|\tau_{i,j}|^2$ associated with the transformation U .

We then move to test the second algorithm based on variance minimization. In Fig. 2(c), we report the measured field intensity in the three outputs of the interferometer for different dissipated powers in one heater, thus corresponding to different evolutions of U , when the signal is injected in input 0. We also report the sum (red curve) of the three intensities for each tested configuration for U . We observe that such a sum is not constant, as one would expect if the output losses were balanced. In Fig. 2(d), we report the same curves after applying the variance minimization algorithm, showing that the application of the algorithm makes the sum constant with respect to changes in the internal transformation. We repeat the same procedure of the previous paragraph by tuning the output mode-dependent losses, showing the capability of retrieving the correct moduli values. The average fidelity, among the same set of N internal operations, between the reconstructed distributions in the two different conditions of losses after the application of the algorithm is $\bar{F} = 0.9996 \pm 0.0002$ ($F_{\min} = 0.9990$). As a further confirmation, we compared the distributions, corresponding to the same optical circuit settings, retrieved by the application of the two algorithms. The mean fidelity between the reconstructed matrix with the two methods is $\bar{F} = 0.999 \pm 0.001$ ($F_{\min} = 0.992$), thus confirming the effectiveness of both algorithms.

Finally, we tested the measurement of the cross-correlations defined in Eq. (16) for the phase reconstruction. Since the phase fluctuations of the fibers do not fulfill the conditions of Eq. (17), we placed a liquid crystal in one arm before the first input of the photonic chip. For the phase modulation, we used a discrete set of phases instead of a continuous one. In particular, we employed the set $\{0, 2\pi/3, 4\pi/3\}$. After recording the temporal fluctuations of the output field intensities, we calculated the normalized cross-correlations for various configurations of the interferometer (red dot in Fig. 3). These measurements are compared with the predictions made by an independent characterization of the device via a white-box algorithm, used as a reference to test our approach. By this alternative method, which exploits the structure of the two tritters, the moduli and the phases of the matrix are retrieved directly from the field intensity distributions of the previous paragraph. It follows that, in this white-box approach used as a reference, the cosines of the internal phases are the result of a numerical optimization between the parameters of the optical circuit, which is designed

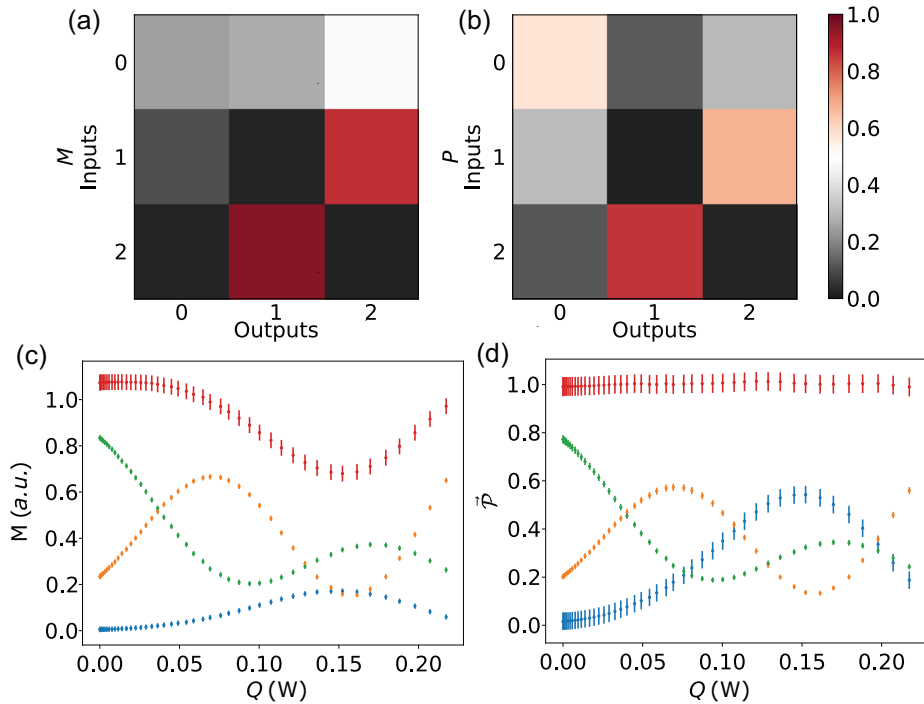


Fig. 2 Losses and moduli estimation. We show the results of the Sinkhorn- and variance minimization-based algorithms. First, we compare the matrix of the field intensities M (a) with the matrix P after the application of the Sinkhorn's algorithm (b). (c) We report the output intensity distribution at the three output ports when the laser is injected in the first input for different values of the electrical powers dissipated in the resistor R_1 . Red points correspond to the sum of the three intensities in the outputs (blue, output port 0; orange, output port 1; and green, output port 2). (d) We report the distribution \bar{P} and the sum after the application of the variance minimization algorithm. The error bars reported in (c) correspond to the precision of the field intensity measurements performed by a power meter. They are propagated to estimate the error of the sum. The error bars in (d) are the result of a Monte Carlo approach applied to the reconstruction algorithm.

according to the structure in Fig. 1(c) and the measurements of the \bar{P} distributions. The blue curve in Fig. 3 represents the prediction of such an optimization. We observe that the direct measurement of cross-correlation via the proposed approach with

classical light and the same quantities retrieved via the white-box method are compatible with the experimental error, with a normalized $\chi^2 = 1.09$. As a final comparison, we compute the fidelity between the second column of the matrix retrieved

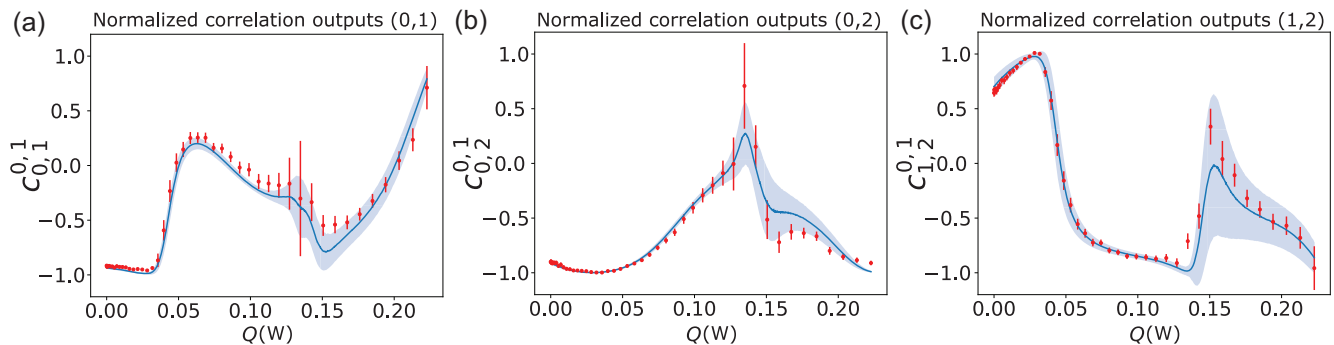


Fig. 3 Cross-correlation measurements. We report the measurement of the normalized cross-correlations C_{ij}^{hk} for different pairs of outputs, entering from $(h, k) = (0, 1)$. In particular, we measure the pairs (a) (0, 1), (b) (0, 2), and (c) (1, 2). We report the experimental correlations for different configurations of the dissipated electrical power in the heater R_1 as in red. The predictions according to the results of a white-box fit that makes use of the structure of the interferometer and the previous measurements of the matrix moduli as in blue. The two independent estimations are in good agreement within one standard deviation of the experimental error.

via our black-box algorithm (bb) U_{i1}^{bb} and the column of the white-box approach (wb) U_{i1}^{wb} . We choose the second column of the matrix, since it presents nontrivial phases, namely, $\phi_{i1} \neq 0$ for $i > 0$. Indeed, the first row and column are imposed to be real vectors because of the equivalence between U and $U' = F_1 U F_2$ with F_1 and F_2 unitary diagonal matrices. The fidelity defined here as $\mathcal{F} = |\sum_{i=0}^2 U_{i1}^{\text{bb}}(U_{i1}^{\text{wb}})^*|^2$, i.e., the overlap between pure single-photon states described by the second column of U , has been estimated for each configuration of the dissipated power in R_1 reported in Fig. 3. The average fidelity is $\bar{\mathcal{F}} = 0.999 \pm 0.001$ ($\mathcal{F}_{\text{min}} = 0.994$).

5 Discussion

In this work, we presented algorithms to characterize the operation of multimode linear optical circuits. In particular, we have shown the possibility of reconstructing the moduli of the unitary matrix element by field intensity measurements, in the presence of unbalanced losses at the input and output ports. This is in contrast to the previous black-box algorithms^{28,29} that can reconstruct the moduli of the matrix only after phases measurements via HOM visibility and by imposing the constraint to have a unitary matrix. In addition, our procedure can provide directly the differential losses among the waveguides at the input and output. We also proposed a method to characterize the internal matrix phases based on intensity correlations of coherent light beams at the outputs of the linear network. These measurement methods do not require knowledge of the matrix moduli and of input/output losses. These approaches enable the possibility of characterizing separately the moduli and the phases of the unitary matrix implemented by the optical network with a reliable and independent approach. Furthermore, all presented algorithms are polynomial in the number of modes of the interferometer, both for the execution time and for the number of measurements required, sharing the same scaling of previous state-of-the-art algorithms. This property makes our algorithms suitable for adaption to large-scale interferometers. An open issue regards the inclusion of unbalanced internal losses in the model. Some recent works have proposed some solutions for taking into account such sources of noise in the U reconstruction.⁴¹ We foresee as a future purpose of our work to adopt the same strategy of independent estimations of moduli and phases to detect the effects of such imperfections. We provided experimental proof of the effectiveness of the algorithm by verifying its performance on a three-mode reconfigurable integrated optical circuit. In this analysis, we compared the results with the predictions of an independent reconstruction that exploits the knowledge of the internal structure of the circuit, which may be in general unknown or too complex to model when taking into account noise processes.

Our findings pave the way for the successful adoption of such an effective black-box methodology to large-scale optical networks, which nowadays are approaching a high number of optical modes and components,^{19,22,23} with applications ranging from quantum communication and sensing to quantum computation and simulation via photonic systems.

Acknowledgments

This work was supported by the European Union's Horizon 2020 research and innovation program through the FET project Photonic Quantum Sampling machine (Grant Agreement No. 899544) and Ministero dell'Istruzione, dell'Università e

della Ricerca via Project PRIN 2017 Taming Complexity via Quantum Strategies a Hybrid Integrated Photonic approach (Id No. 2017SRNBRK). The authors declare no competing financial interests.

References

1. K. Vandoorne et al., "Experimental demonstration of reservoir computing on a silicon photonics chip," *Nat. Commun.* **5**, 3541 (2014).
2. D. Brunner, M. C. Soriano, and G. V. der Sande, Eds., *Photonic Reservoir Computing: Optical Recurrent Neural Networks*, De Gruyter (2019).
3. M. Rafayelyan et al., "Large-scale optical reservoir computing for spatiotemporal chaotic systems prediction," *Phys. Rev. X* **10**, 041037 (2020).
4. M. Nakajima, K. Tanaka, and T. Hashimoto, "Scalable reservoir computing on coherent linear photonic processor," *Commun. Phys.* **4**, 20 (2021).
5. Y. Shen et al., "Deep learning with coherent nanophotonic circuits," *Nat. Photonics* **11**, 441–446 (2017).
6. T. Wang et al., "An optical neural network using less than 1 photon per multiplication," *Nat. Commun.* **13**, 123 (2022).
7. D. Pierangeli, G. Marcucci, and C. Conti, "Large-scale photonic Ising machine by spatial light modulation," *Phys. Rev. Lett.* **122**, 213902 (2019).
8. Y. Okawachi et al., "Demonstration of chip-based coupled degenerate optical parametric oscillators for realizing a nanophotonic spin-glass," *Nat. Commun.* **11**, 4119 (2020).
9. M. Leonetti et al., "Optical computation of a spin glass dynamics with tunable complexity," *Proc. Natl. Acad. Sci. U. S. A.* **118**(21), e2015207118 (2021).
10. F. Flamini, N. Spagnolo, and F. Sciarrino, "Photonic quantum information processing: a review," *Rep. Progr. Phys.* **82**, 016001 (2018).
11. J. Wang et al., "Integrated photonic quantum technologies," *Nat. Photonics* **14**, 273–284 (2020).
12. M. Gräfe et al., "Integrated photonic quantum walks," *J. Opt.* **18**, 103002 (2016).
13. F. Cardano et al., "Quantum walks and wavepacket dynamics on a lattice with twisted photons," *Sci. Adv.* **1**(2), e1500087 (2015).
14. C. Esposito et al., "Quantum walks of two correlated photons in a 2D synthetic lattice," *NPJ Quantum Inf.* **8**, 34 (2022).
15. J. Wang et al., "Experimental quantum Hamiltonian learning," *Nat. Phys.* **13**, 551–555 (2017).
16. V. Saggio et al., "Experimental quantum speed-up in reinforcement learning agents," *Nature* **591**, 229–233 (2021).
17. M. Spagnolo et al., "Experimental photonic quantum memristor," *Nat. Photonics* **16**, 318–323 (2022).
18. H.-S. Zhong et al., "Quantum computational advantage using photons," *Science* **370**(6523), 1460–1463 (2020).
19. H.-S. Zhong et al., "Phase-programmable Gaussian boson sampling using stimulated squeezed light," *Phys. Rev. Lett.* **127**, 180502 (2021).
20. L. S. Madsen et al., "Quantum computational advantage with a programmable photonic processor," *Nature* **606**, 75–81 (2022).
21. E. Pelucchi et al., "The potential and global outlook of integrated photonics for quantum technologies," *Nat. Rev. Phys.* **4**, 194–208 (2022).
22. C. Taballione et al., "20-mode universal quantum photonic processor," arXiv:2203.01801 (2022).
23. F. Hoch et al., "Reconfigurable continuously-coupled 3D photonic circuit for boson sampling experiments," *NPJ Quantum Inf.* **8**, 35 (2021).
24. M. Reck et al., "Experimental realization of any discrete unitary operator," *Phys. Rev. Lett.* **73**, 58–61 (1994).
25. W. R. Clements et al., "Optimal design for universal multiport interferometers," *Optica* **3**, 1460–1465 (2016).

26. M. Tillmann, C. Schmidt, and P. Walther, "On unitary reconstruction of linear optical networks," *J. Opt.* **18**, 114002 (2016).
27. N. Spagnolo et al., "Learning an unknown transformation via a genetic approach," *Sci. Rep.* **7**, 14316 (2017).
28. A. Laing and J. L. O'Brien, "Super-stable tomography of any linear optical device," arXiv:1208.2868 (2012).
29. I. Dhand et al., "Accurate and precise characterization of linear optical interferometers," *J. Opt.* **18**, 035204 (2016).
30. S. Rahimi-Keshari et al., "Direct characterization of linear-optical networks," *Opt. Express* **21**, 13450–13458 (2013).
31. S. M. Popoff et al., "Measuring the transmission matrix in optics: an approach to the study and control of light propagation in disordered media," *Phys. Rev. Lett.* **104**, 100601 (2010).
32. S. M. Popoff et al., "Controlling light through optical disordered media: transmission matrix approach," *New J. Phys.* **13**, 123021 (2011).
33. D. Suess et al., "Rapid characterisation of linear-optical networks via PhaseLift," arXiv:2010.00517 (2020).
34. V. Cimini et al., "Calibration of multiparameter sensors via machine learning at the single-photon level," *Phys. Rev. Appl.* **15**, 044003 (2021).
35. A. Suprano et al., "Dynamical learning of a photonics quantum-state engineering process," *Adv. Photon.* **3**(6), 1–11 (2021).
36. S. Kuzmin, I. Dyakonov, and S. Kulik, "Architecture agnostic algorithm for reconfigurable optical interferometer programming," *Opt. Express* **29**, 38429–38440 (2021).
37. C.-K. Hong, Z.-Y. Ou, and L. Mandel, "Measurement of subpicosecond time intervals between two photons by interference," *Phys. Rev. Lett.* **59**(18), 2044–2046 (1987).
38. R. Keil et al., "Photon correlations in two-dimensional waveguide arrays and their classical estimate," *Phys. Rev. A* **81**, 023834 (2010).
39. R. Hanbury Brown and R. Q. Twiss, "A test of a new type of stellar interferometer on Sirius," *Nature* **178**, 1046–1048 (1956).
40. M. Oszmaniec and D. J. Brod, "Classical simulation of photonic linear optics with lost particles," *New J. Phys.* **20**, 092002 (2018).
41. S. Rahimi-Keshari, S. Baghbanzadeh, and C. M. Caves, "In situ characterization of linear-optical networks in randomized boson sampling," *Phys. Rev. A* **101**, 043809 (2020).
42. R. Sinkhorn and P. Knopp, "Concerning nonnegative matrices and doubly stochastic matrices," *Pac. J. Math.* **21**, 343–348 (1967).
43. R. Sinkhorn, "Continuous dependence on A in the D_1AD_2 theorems," *Proc. Am. Math. Soc.* **32**(2), 395–398 (1972).
44. M. Idel, "A review of matrix scaling and Sinkhorn's normal form for matrices and positive maps," arXiv:1609.06349 (2016).
45. R. R. Gattass and E. Mazur, "Femtosecond laser micromachining in transparent materials," *Nat. Photonics* **2**(4), 219–225 (2008).
46. N. Spagnolo et al., "Three-photon bosonic coalescence in an integrated tritter," *Nat. Commun.* **4**, 1606 (2013).
47. E. Polino et al., "Experimental multiphase estimation on a chip," *Optica* **6**, 288–295 (2019).

Francesco Hoch received his master's degree in 2019. He is currently a PhD student in the Physics Department of Sapienza University. His research interest focuses on reconfigurable integrated optics and their application for quantum information and quantum computation. In particular, he worked on the development of new reconfigurable devices for the boson sampling experiment and the study of the optical implementation of recently proposed quantum protocols.

Taira Giordani received her PhD in physics in 2020. She is currently a postdoc in the Physics Department of Sapienza University. Her research focuses on the experimental implementation of quantum walks in integrated photonic devices and the angular momentum of light. In this context, her efforts aim to develop machine learning and optimization methods for the certification and engineering of photonic quantum walk platforms.

Nicolò Spagnolo received his PhD in 2012 in physical sciences of matter with a thesis on experimental multiphoton quantum optical states. He is currently tenure-track assistant professor in the Physics Department of Sapienza Università di Roma. His research interests are focused on quantum information protocols employing different photonic platforms. These research activities include the implementation of boson sampling instances and of validation protocols with integrated photonics, quantum phase estimation experiments, and optical quantum communications.

Andrea Crespi received his PhD in physics from the Politecnico di Milano, Italy, in 2012. From 2012 to 2016, he worked as a research fellow at the Institute for Photonics and Nanotechnologies of the National Research Council. Since 2016, he has been in the Physics Department of Politecnico di Milano, where he is now an associate professor. His research interests include femtosecond laser micromachining of glass and the development of integrated photonics circuits for quantum photonics applications.

Roberto Osellame received his PhD in physics from the Politecnico di Torino in 2000. He is a research director at the Institute for Photonics and Nanotechnologies of the National Research Council, Milan, Italy. His research interests focus on microfabrication of integrated photonic devices for quantum technologies, lab-on-a-chip, and optical communications. He is a co-author of more than 300 publications and holds 15 patents. He is a fellow of *Optica* and an ERC awardee.

Fabio Sciarrino received his PhD in 2004 with a thesis in experimental quantum optics. He is a full professor and a head of the Quantum Lab in the Department of Physics of Sapienza Università di Roma. Since 2013, he has been a fellow of the Sapienza School for Advanced Studies. His main field of research is quantum information and quantum optics, with works on quantum teleportation, optimal quantum machines, fundamental tests, quantum communication, and orbital angular momentum.